5-5-2023

Isolating the electronic effects of systematic twist in highly substituted aromatic hydrocarbons using density functional theory

Grace Tully
gtully1@lion.lmu.edu

Emily A. Jarvis
Loyola Marymount University, emily.jarvis@lmu.edu

Isolating the electronic effects of systematic twist in highly substituted aromatic hydrocarbons using density functional theory

A thesis submitted in partial satisfaction

of the requirements of the University Honors Program

of Loyola Marymount University

by

Georgia Grace Tully and Emily Jarvis, PhD

May 5th, 2023

Abstract

      Density functional theory (DFT) was employed to investigate dodecaphenyltetracene as well as similar molecules containing differing backbone lengths and electron withdrawing groups with interest in manipulating the twist to lower the LUMO level for increased electron mobility. Optimization and frequency time-independent calculations followed by time-dependent (TD-DFT) energy calculations were performed at the B3LYP/G-311G level of theory to analyze electronic trends as a result of increased backbone length and consequently distorted end-to-end molecular twist. These calculations demonstrate a linear relationship with negative slope between the estimated HOMO-LUMO, fundamental, and optical gaps as a function of the number of fused rings along the polycyclic backbone. Contrasting these energy gaps with a separate series of identical molecules fixed into a planar configuration, the optimized twisted molecules display a pronounced red shift from steric hindrance due to phenyl substituents. In addition to the excitation energies, we applied a theoretical model for predicting exciton binding energy in planar polycyclic aromatic hydrocarbons to our series of twisted analogs, demonstrating a negligible effect of intramolecular twist on exciton binding energy. Evaluating higher levels of theory that incorporate dispersion and solvation effects, we found that our original gas-phase calculations sufficiently capture trends in expected excitation energies.

<u>Introduction</u>

Polycyclic aromatic hydrocarbons (PAHs) are of prominent research interest for a wide range of reasons spanning that these molecules are present as environmental toxins,[1] they possess electronic properties harnessed in breakthrough technological devices,[2-6] and they even form the interstellar dust of our galaxy.[7-9] While a myriad of PAHs have been synthesized for electronic applications, pentacene, an organic molecule comprised of five linearly-fused benzene rings, has been a popular choice small organic semiconductor (OSC) for incorporation into OFETs because of its favorable charge carrier mobility and transport.[10,11] The success of pentacene and its derivatives has sparked interest into synthesizing polyacenes with backbone lengths even larger than five rings to further extend the π-orbital systems. However, these attempts have been largely unsuccessful due to increased instability, unstable phase behavior, and decreased solubility.[12] An alternative method of extending electron delocalization without extending the backbone has been to synthesize polyacene derivatives with phenyl side groups, such as rubrene.[13-15] The unique intramolecular twist of these phenyl-substituted derivatives is of great interest because this geometric feature could induce favorable electronic and optical properties. Understanding the impact of substituents and geometric twist on the electronic states of these classes of molecules could expand incorporation of these inexpensive materials into organic-light emitting diodes (OLEDs),[16-17] organic field-effect transistors (OFETs), and organic photovoltaic (OPV) solar cells.[18-22]

Currently, multiple organic synthesis groups are working to improve the efficiency of synthesizing these phenyl-substituted polycyclic aromatic hydrocarbons as well as develop pathways for novel molecules of this form.[23-28] Additional derivatives of highly twisted PAHs have been developed using bulky, electron withdrawing, and electron donating substituent groups in addition to phenyl substituents to improve solubility in organic solvent for integration into OFETs.[29-33] Experimental analyses on these molecules support previous findings that the twisted geometric structure supports overall stability as well as unique photophysical properties.[34-42] However, understanding the relationship between the twisted geometry of sterically hindered PAHs and its electronic and photophysical properties is more clearly elucidated when analyzing families of OSCs with homogenous substituent groups. In this case, we will focus on isolating the twist effect by analyzing molecules with only phenyl substituents. As a result of adding phenyl substituents to the traditional planar unsubstituted polycyclic aromatic hydrocarbon families such as oligoacenes, phenacenes, circumacenes, and oligorylenes (Figure 1) new families of "twistacenes," a term coined by Robert Pascal, have been introduced as viable alternatives for organic electronic applications (Figure 2).
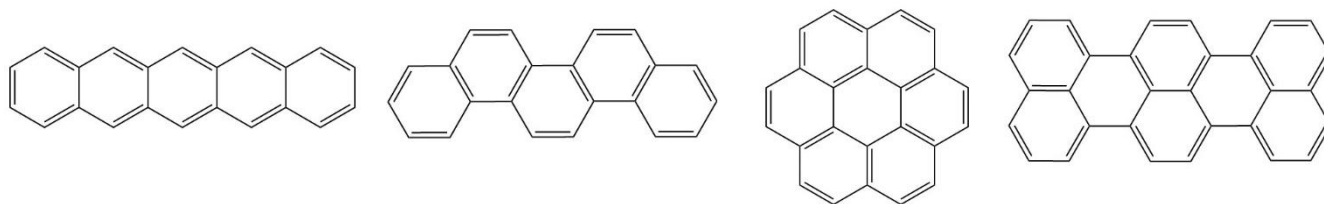

Figure 1: Three different families of planar polycyclic aromatic hydrocarbons from left to right are oligoacenes, phenacenes, circumacenes, and oligorylenes. The oligoacene family are the parent molecules for our investigation.

Previous experimental and theoretical techniques have been applied to isolate electronic effects of twist from geometric effects. Our theoretical approach closely resembles that applied by Norton *et al* who used Density Functional Theory (DFT) to analyze the electronic structure of twistacenes.[43] They focused on Pascal's synthesis of a pentacene exhibiting a 144° twist as well as a model system consisting of an identical backbone in bond length and twist deviation but lacking the six interior phenyl substituents. They concluded that typical electronic features of polyacenes, such as end-to-end electron delocalization, are unaffected by the twisting of the backbone. Bedi et al. came to the same conclusion using a model system to computationally investigate the effect of twisting on polyacenes from two to five benzene rings in length, varying the degree of twist by ten degrees from 0 - 30°. He reported a similar insignificant decrease in the HOMO-LUMO gap as a result of twist, while adding that the energy gap between the singlet ground state and the lowest triplet state (ΔE_{TS}) also slightly decreased as a result of increased intramolecular twist.[44] Bedi also experimentally isolated the effect of twisting by synthesizing a series of anthracene molecules with a carbon tether of various lengths across the molecule and reported a similar decrease in HOMO-LUMO gap, as well as decreased fluorescence quantum efficiency, likely due to increased spin orbit coupling.[45]

While these generic model systems have provided valuable insight into the effect of steric-induced intramolecular twisting, there has yet to be a systematic investigation into the electronic properties of the series of twisted polyacenes that have been synthesized by Pascal *et al*. In this computational investigation, we build upon previous work by investigating the electronic properties of fully phenyl substituted polyacenes (Series 1), partially phenyl substituted polyacenes (Series 2), and the alternately fused phenyl-substituted series recently synthesized by Clevenger *et al*.(Series 3).[46] In addition, we also investigated a model system using an identical steric-induced twist of Series 1, but with hydrogens in place of the phenyl substituents (Series 4). Here we provide a quantitative review of electronic properties as well as qualitative analysis of the molecular orbitals as a result of intramolecular twist.
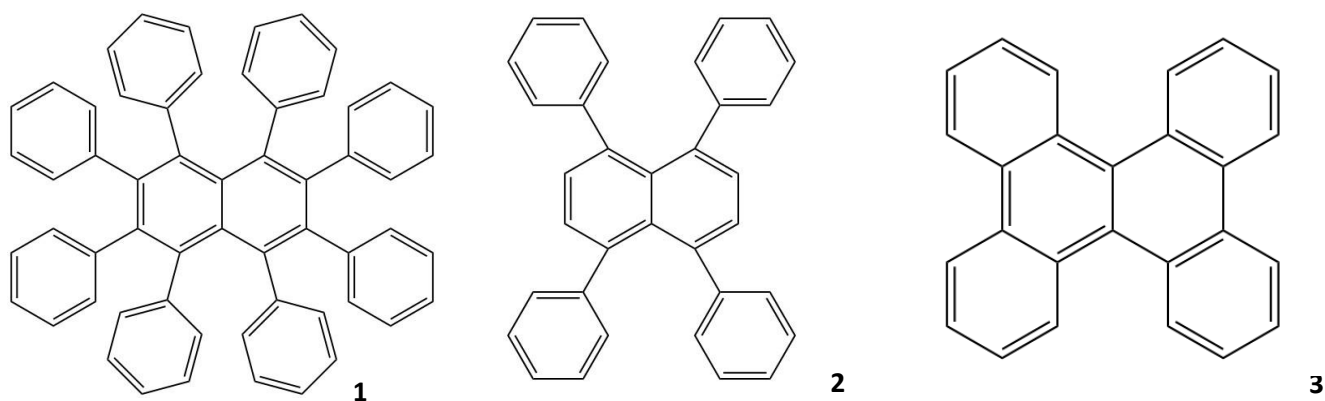

Figure 2: Three different twistacene series were investigated with backbone lengths n=2 to n=7. The smallest molecule in each series (n=2) is depicted above.

Computational Details

Geometry optimization

We optimized the geometries of all molecules in Series 1-4 using the hybrid B3LYP[47-50] functional with the 6-311G basis set, which has been demonstrated to accurately predict the ground-state properties of PAHs. For molecules with backbone length 2-4 in Series 1, we also optimized the molecules using the conductor-like polarizable continuum model, CPCM,[51] with cyclohexane as the solvent represented as a dielectric polarizable continuum. Cyclohexane was chosen to correspond with available experimental data. We also calculated optimized geometries of the Pascal series using the more robust long-range corrected CAM-B3LYP functional.[52] We focused on these particular derivatives of the Pascal series for additional optimization calculations because they have been synthesized and analyzed so present available experimental data with which to benchmark our calculations.

Electronic properties

We explored the electronic properties of our π-conjugated molecular systems by analyzing the excitation and ionization energies of the molecules related to the difference in energy between the highest occupied molecular orbital (HOMO) and the lowest occupied molecular orbital (LUMO). We compared the calculated HOMO-LUMO gap, fundamental gap, optical gap, and difference between the HOMO energy of the molecule in the ground state and the HOMO of the N+1 electron system. The HOMO-LUMO gap is the difference between the HOMO energy and LUMO energy provided by the one-electron wavefunctions on the neutral, ground-state molecular system. The HOMO-LUMO gap approximates the fundamental gap, which is the difference between the ionization potential and electron affinity, rigorously defined by the following equation: $E_{fund} = IE_v - EA_v = (E_{N-1} - E_N) - (E_N - E_{N+1})$.[53-55] The anion and cation energies were calculated in the ground state using the previously optimized neutral geometries. We used the differences between the HOMO-LUMO and fundamental gap energies to evaluate the suitability of our chosen exchange-correlation functional and basis set. The optical gap was given from the wavelength associated with the lowest absorption electronic transition (S_0 to S_1) from the TD-DFT energy calculation of each molecule in the excited state. The difference between the fundamental gap and the optical gap describes the exciton binding energy, or energy associated with the electron and hole in the excited state as opposed to the free electron in the ionized state. We evaluated the relationship between backbone length of our series of molecules with a previous theoretical description of exciton binding energy as proportional to the inverse of the radius of planar PAHs, $BE \approx e^2/(4\pi\varepsilon_0\varepsilon R)$. All excitation energies are reported in units of electron volts (eV). [56]
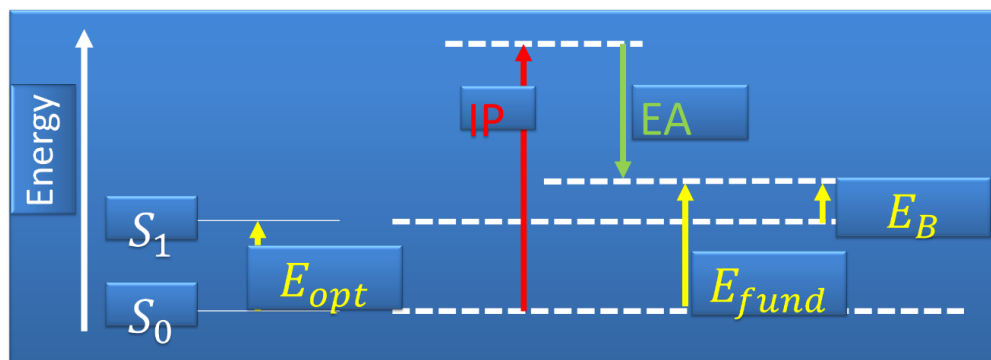

Figure 3: Influenced by Bredas' 2014 article *Mind the Gap*!, this diagram further displays the difference between the various calculations of the excitation energies that we explored.

Optimized structures

We quantified the degree of end-to-end molecular twist unique to these molecules' backbone structures arising from steric effects of phenyl substitution. This is defined by the torsion angles, either $\angle 1234$ or $\angle 2143$ depending on twist direction, that span between both ends of the backbone as represented in Figure 4.
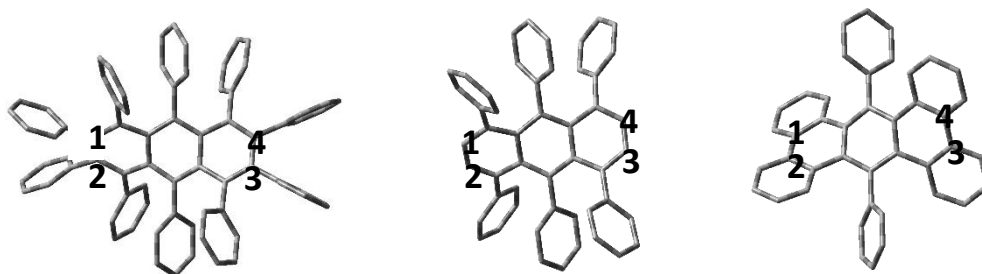

Figure 4: Labeled carbon positions for defining the torsion angles of interest for Series 1,2, and 3 from left to right for the example of the three-ring backbone derivative.

The degree of end-to-end molecular twist increases linearly with as the backbone length increases with R^2 values of 0.9715, 0.9749, and 0.9471 for Series 1-3 respectively (Figure 5a). The increase in end-to-end torsion angle above 180 °as the backbone increases in length from six to seven benzene rings represents the molecule twisting upon itself as the last backbone ring fragment comes into plane with the first ring fragment (Figure 5b).
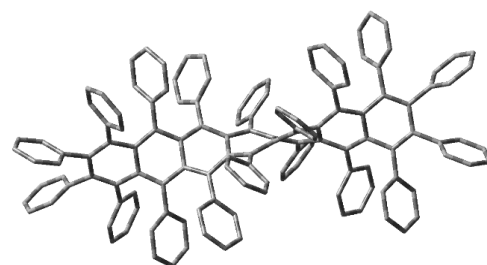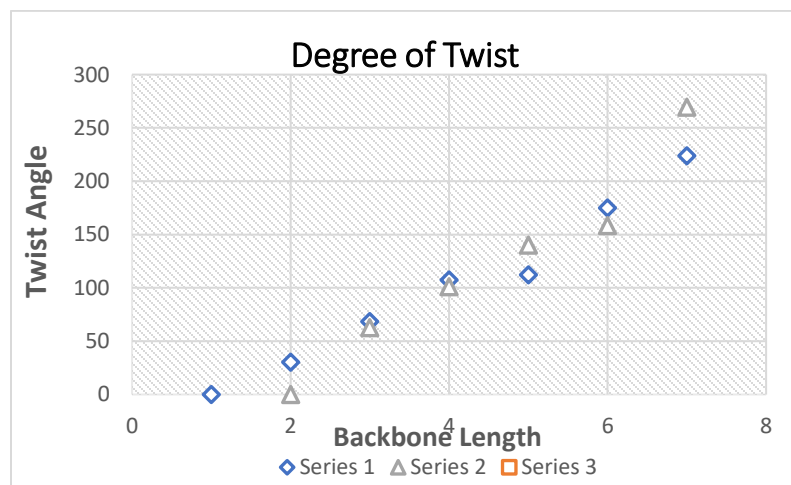

Figure 5: a) The end-to-end torsion twist angle as a function of the length of the backbone in benzene ring fragments for Series 1,2, and 3. b) The optimized structure for the seven-ring backbone derivative of the Pascal series (not yet synthesized) demonstrating that a possible end-to-end 360° twist will emerge as longer derivatives or chains of twisted PAHs are developed.

While the end-to-end twist is significant, individual bond angle deviations from the theoretical 120° in an sp2 hybridized planar PAH are minor. For example, in the optimized structure of the largest molecule in Series 1 as seen in Figure 2b, individual bond angles between carbons on the backbone range from 115 - 128°, with the average hovering around 120°. Experimental X-ray diffraction data is available in the solid state for molecules 1-4 of Series 1 and 2-5 of Series 3.

Table 1: Series 3 computed torsion angles compared with x-ray diffraction torsion angles and calculations computed by Clevenger *et al.*

Backbone length	BY3LP/6-311G	X-ray diffraction	Clevenger calculated
2	37.45597	--	--
3	70.91131	66	>60 (MMPI)
4	108.09458	105	109 (B3LYP/6-31G9(d))
5	120.7508	144	143 (AM1)
6	172.59529	184	182 (AM1)
7	132.38536	--	220 (AM1)

Table 2: Series 1 torsion computed angles compared with x-ray diffraction torsion angles identified by Pascal *et al.* which are also defined by Figure 5.

Backbone length	BY3LP/6-311G	X-ray diffraction
1	0.003	0
2	30.26223	31
3	68.36581	62.8
4	107.406	97

Our DFT optimized geometries (B3LYP with 6-311G) capture the same trends seen in x-ray diffraction results for Series 3 and Series 1 shown in Table 1 and Table 2, respectively. We expected minor variation between our optimized structures in gas phase and the experimental solid-state crystal structures due to the intermolecular interactions in the different phase environments.

Supported by previous experimental and theoretical studies, the end-to-end molecular twist has minor effects on overall electron delocalization. As seen in Figure 6, the Series 1 HOMO and LUMO orbitals from the optimized calculations remain mostly centralized along the fused backbone, with minor sections of localized electron density spreading to substituent phenyl groups. The similarity in the molecular orbital characteristics of the Series 1 derivatives with their planar parent molecules suggests that electronic behavior in material applications would also be similar.
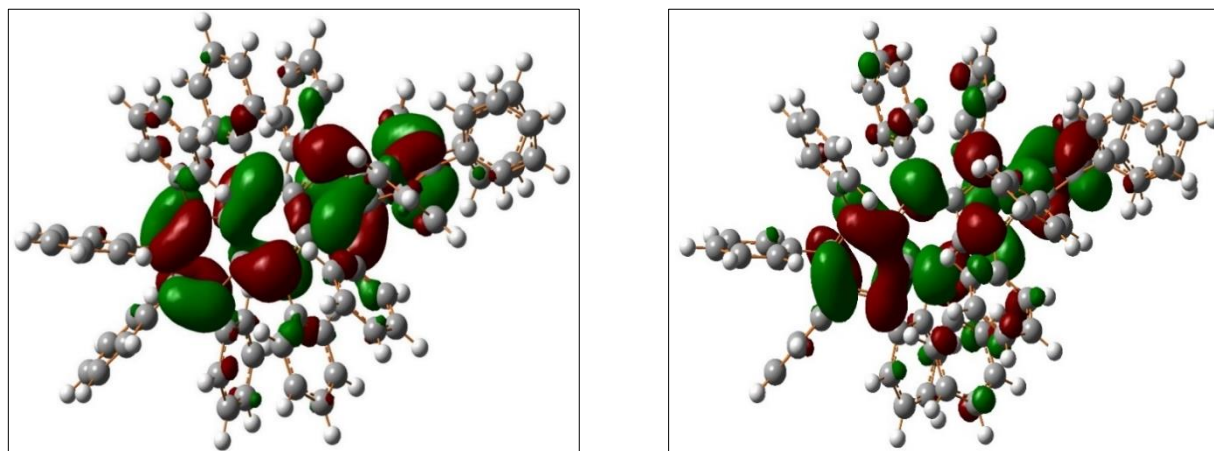

Figure 6: The HOMO and LUMO of the optimized structure of dodecaphenyltetracene calculated with the B3LYP functional at the 6-311G level of theory.

For the Series 3 molecules, there is generally more electron density distributed to the side phenyl groups (Figure 7). However, this trend decreases as the length of molecule increases: the six-ring backbone derivative has essentially all the electron density located on the backbone itself. Series 2 molecules showed a similar trend to Series 1, but with some LUMOs spread extensively into the substituent regions. Bond lengths between the optimized geometries of all molecules analyzed were the same as their planar parent molecules, averaging around 1.41 angstroms.
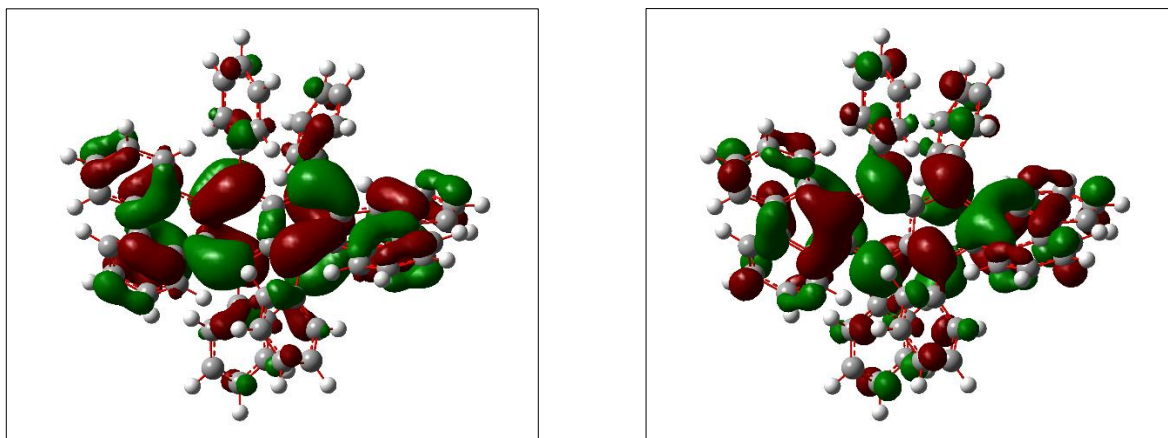

Figure 7: The HOMO and LUMO of the optimized structure of dodecaphenyltetracene calculated with the B3LYP functional at the 6-311G level of theory.

Minor differences in optimized structures of molecules 1-4 in cyclohexane using CPCM solvation model were observed.

Fundamental, HOMO-LUMO, and Optical Excitation Energies

The calculated values for the HOMO-LUMO gap, optical gap, and fundamental gap are displayed along with the three experimental UV-vis absorption wavelengths measured in cyclohexane for Series 1 in Figure 8. The time-dependent UV-vis absorption wavelengths for molecules 2-4 show excellent agreement with the experimental values, with 5.1, 6.0, and 2.5 % differences respectively.[57] Both the experimental and theoretical UV-vis absorption spectra show broad absorption peaks corresponding to excitation in the lowest singlet state (S_0 to S_1). The general linear decrease in excitation energies relative to the increase in backbone ring length is expected for an increase size of a π-conjugated system, demonstrating that the increase in intramolecular twist does not affect overall electron delocalization.
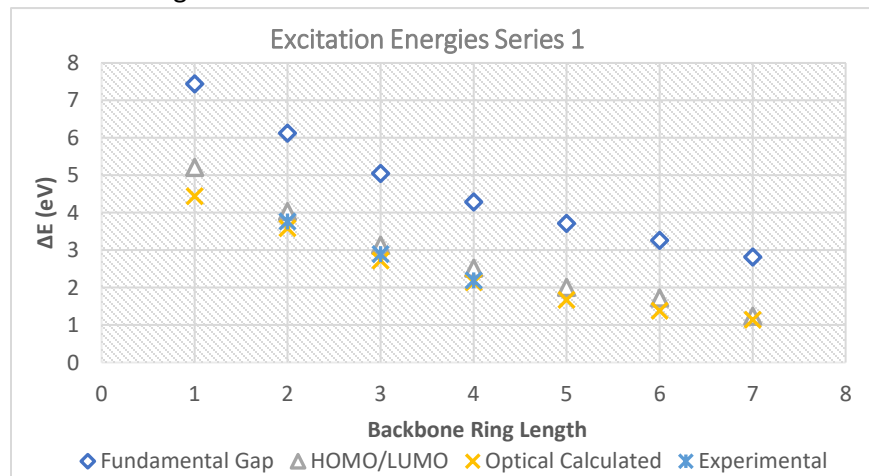

Figure 8: The B3LYP/6-311G fundamental gap, HOMO/LUMO gap, and optical gap (TD) for Series 1 compared with UV-vis 1st singlet excitation energies for molecules 2-4. [57]

Similar trends showing expected decrease in excitation energies with increasing size of the molecular backbone are also reflected in the Series 2 calculations (Figure 9). One exception is an outlier in the HOMO-LUMO gap for four-ring backbone derivative. While we are still looking into reasons to explain the outlier, one contributing cause could be the difference in the LUMO molecular orbital. Unlike the LUMOs of the other molecules in the series which extend widely into the side phenyl substituent groups, the four-ring molecule's LUMO is tightly packed around the backbone. There is no evidence in the literature of the synthesis of Series 2 molecules so there is no experimental data to compare the excitation energies.
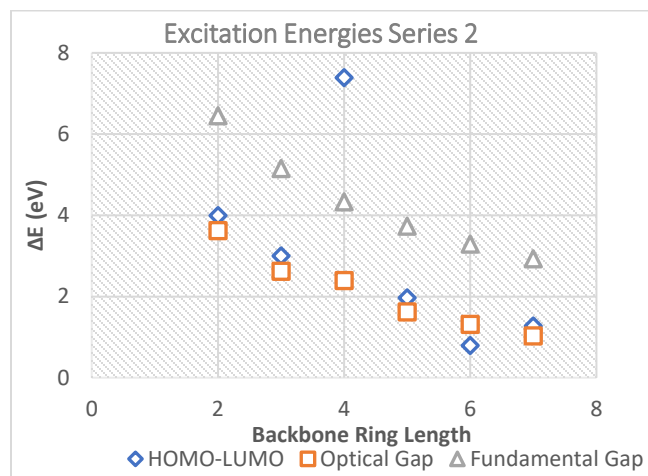

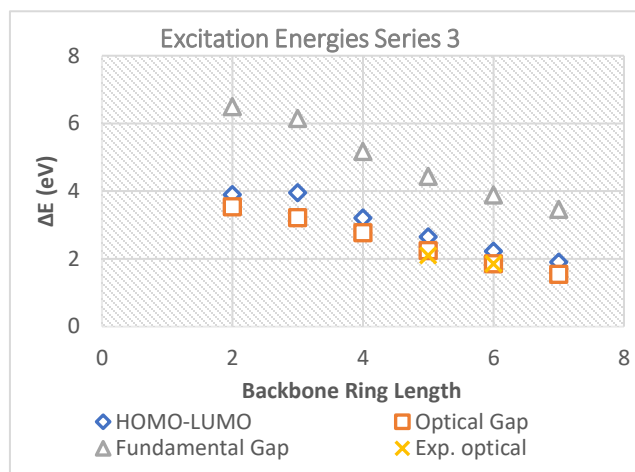Figure 9: The fundamental gap, HOMO-LUMO gap, and optical gap (TD) for Series 2.

Figure 10: The fundamental gap, HOMO-LUMO gap, and optical gap (TD) for Series 1 compared with UV-vis 1st singlet excitation energies for molecules 5 and 6.

The excitation energies in Series 3 follow the trends for Series 1 and 2, supporting the conclusion that twisting does not disrupt end-to-end electron delocalization in conjugated systems (Figure 10). The two optical gap experimental values for molecules 5 and 6 in Series 3 were measured in $CHCl_3$, and our theoretical measurements differed by only 6.4% and 0.47%, respectively. [58,46] Not included in Figure 10 is an experimental HOMO-LUMO gap value determined using cyclic voltammetry for molecule 6 of Series 3 of 2.14 eV which is within 4.41% of our calculated value.[46]

Exciton Binding Energy:

We compared the calculated exciton binding energy (E_{fund} − E_{opt}) to the theoretical calculation previously developed by Nayak $E_{bind} \approx e^2/(4\pi\varepsilon_0\varepsilon R)$ used for planar PAHs.[56] Using the general relationship of BE = C*(1/R), with C = $e^2/(4\pi\varepsilon_0\varepsilon)$, we calculated C for each theoretical E_{bind} using the molecular bond distance between the two farthest hydrogen atoms on phenyl substituents as R (Figure 11). The average value of C was determined to be 42.7 ± 2.9. Using C, we calculated a theoretical E_{BT} for each molecule in the series. We performed the same methods to calculate the exciton binding energies for the planar PAH derivatives:
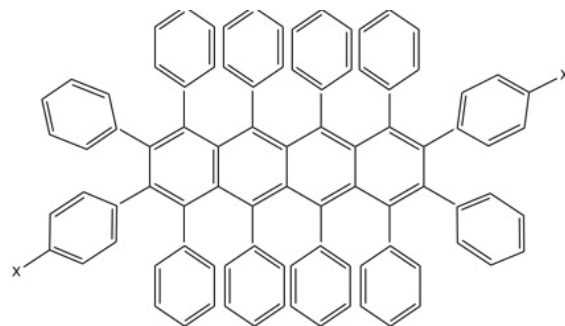

Figure 11: The molecular radius R incorporated in $E_{bind} \approx e^2/(4\pi\varepsilon_0\varepsilon R)$ is the distance between both hydrogen atoms labelled "x" in this 2D figure of dodecaphenyltetracene (Series 1, molecule 4).

naphthalene, anthracene, tetracene, pentacene, hexacene, and heptacene. Using the average C value, 6.14 ± 1.38, we compared E_{bind} with E_{BT}.

Table 3: Displaying the exciton binding energy (E_{Bind}), molecular radius (R), theoretical constant (C), theoretical exciton binding energy (E_{BT}), and the percent difference between E_{Bind} and E_{BT}. All data have been obtained at the B3LYP/6-311G level of theory.

Backbone Ring Length	E_{bind}	R	C	E_{BT}	% Diff
1	3.00	13.63	40.87	3.13	4.36
2	2.54	15.57	39.58	2.74	7.36
3	2.32	17.33	40.19	2.47	5.93
4	2.15	19.22	41.23	2.22	3.50
5	2.04	22.47	45.86	1.90	7.33
6	1.88	24.68	46.51	1.73	8.84
7	1.68	26.74	44.85	1.60	4.98
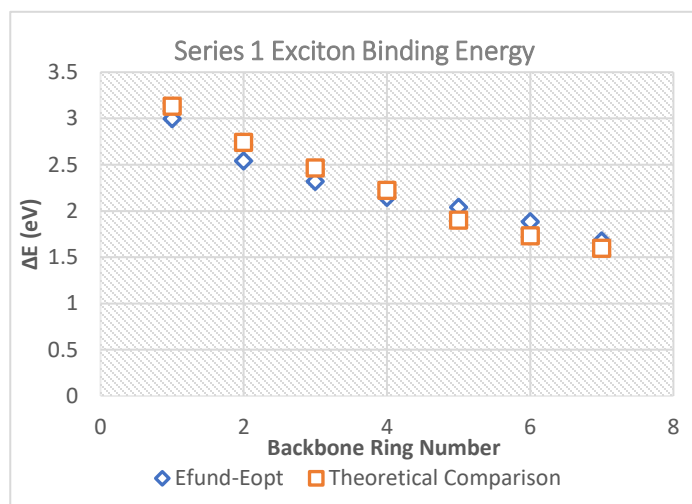
Figure 12: The exciton binding energy (E_{bind}) along with the theoretical relationship $E_{bind} \approx e^2/(4\pi\varepsilon_0\varepsilon R)$ used previously in planar PAHs.
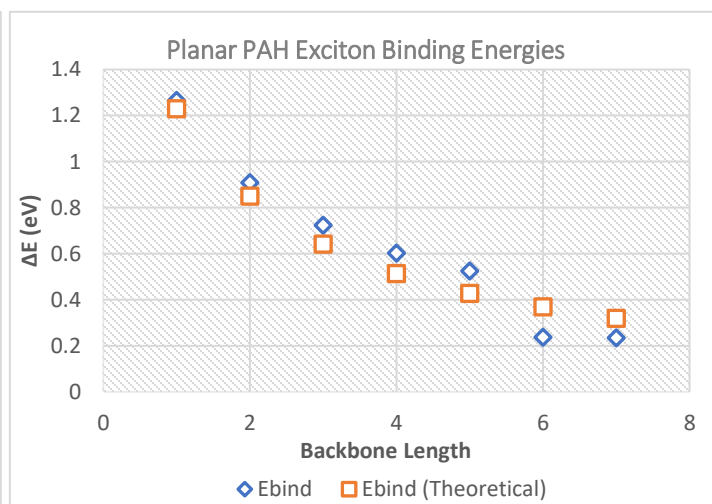
Figure 13: The exciton binding energy (E_{bind}) along with the theoretical relationship $E_{bind} \approx e^2/(4\pi\varepsilon_0\varepsilon R)$ applied for our B3LYP/6-311G calculations on linearly fused PAHs (naphthalene- heptacene).

As seen in Figures 12 and 13, the calculated exciton binding energies for Series 1 follow the relationship of $E_{bind} = C/R$, suggesting that the intramolecular twist does not affect predicted exciton binding energies in small molecule organic semiconductors.

Isolating the Twist:

We used two sets of model systems to isolate the effect of twist from substituent effect on the excitation energies in the Series 1 molecules. The first set of model systems was developed by constraining the backbone geometries of the Series 1 derivatives to a planar configuration leaving the phenyl groups attached perpendicular to the backbone (Figure 14).
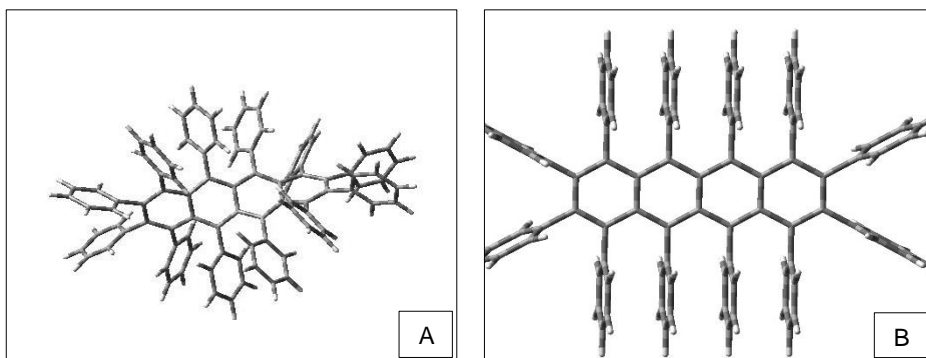
Figure 14: Optimized twisted form of dodecaphenyltetracene (A) adjacent to the geometrically constrained form that maintains planarity of the fused ring backbone (B).

After constraining the molecule to its planar configuration, we were able to calculate their HOMO-LUMO and optical gaps. In the case of these molecules with inherent locked-in strain, the HOMO and LUMO orbitals showed localization adjacent to the backbone along the stacked phenyl substituent groups. Visualizing the molecular orbitals in Gaussview, we instead selected the appropriate orbitals near the HOMO-LUMO that represented the ones with localized along the molecular backbone. The difference between these calculated HOMO-LUMO gaps and the optimized HOMO-LUMO gaps are displayed in Figure 15.

Figure 15: The relationship between the backbone length of the twisted aromatic hydrocarbons and the approximated fundamental gap showing the results for the constrained (blue) and twisted (red) geometric configurations.

It is expected that the optimized configuration of any molecule is its lowest energy configuration which would be reflected in lower energy molecular orbitals. However, the red shift fr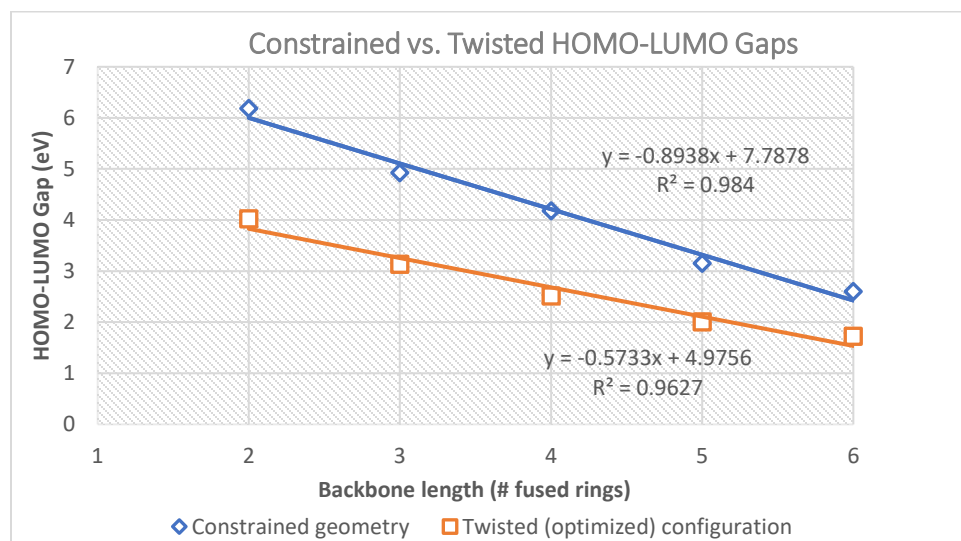om the constrained to twisted geometric configuration is significant considering magnitude and that the HOMO-LUMO orbitals investigated were localized primarily along the backbone in both instances. This suggests that the twisting π-conjugated systems does not negatively impact the frequently desired low excitation energies for OSC applications. Alternatively, the significant redshift could suggest that small molecule OSCs with twisted geometries could possess HOMO-LUMO excitation energies lower than what would be predicted if they were planar.

The second set of model systems we investigated were designed by replacing the phenyl substituent groups from the optimized Series 1 derivatives with hydrogen (Figure 16). We then calculated the HOMO-LUMO excitation energies on these molecules and compared them to the planar PAH parent molecules.
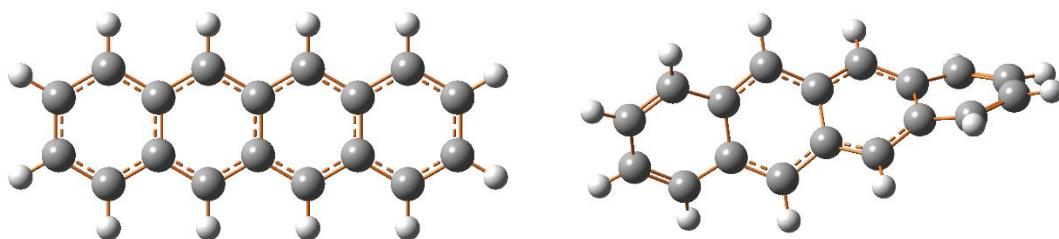
Figure 16: The planar PAH tetracene (left) and the twisted tetracene model system (right).
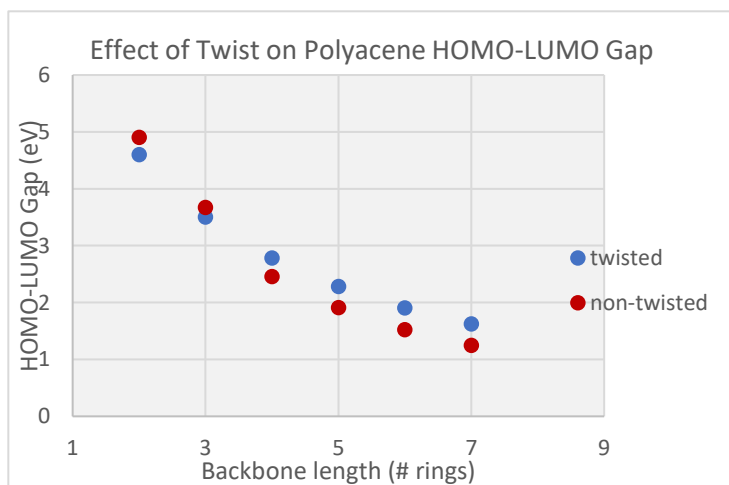
Figure 17: The relationship between the backbone length of the twisted tetracene with hydrogen substituents and the HOMO-LUMO gap showing the results for the twisted fused backbone and the non-twisted, optimized geometric configurations.

Table 4: The absolute difference (Δ)and percent difference between the HOMO-LUMO gap of twisted and untwisted molecules in the model series.

	Δ	% Diff
2	0.3031	6.591
3	0.1706	4.871
4	0.3233	11.616
5	0.3725	16.321
6	0.3793	19.920
7	0.3791	23.326

The HOMO-LUMO gaps for the smaller derivatives of backbone lengths 2 and 3 are slightly lower in energy from the natural structure, which is somewhat surprising considering we would expect optimized structures to have lower total energy and correspondingly, lower energy molecular orbitals. The average difference in eV between the HOMO-LUMO gaps of the twisted and untwisted configurations (Δ_{avg}) is

0.3213 eV. The HOMO-LUMO gap decreases with increasing molecular size and the corresponding Δ does not decrease. This results in an increase in percent difference between the planar and twisted HOMO-LUMO excitation energies (Table 4).

Evaluating dispersion and solvation effects

Often long-range corrected functional groups are applied for calculating excitation energies of large organic molecules due to the possibility of intrinsic dispersion effects. To address the possibility of these dispersions affecting the electronic behavior of our large molecular series, we also calculated the fundamental and optical gaps of Series 1 derivatives using the CAM-B3LYP functional.

Additionally, in device applications, these molecules are incorporated into OFETs by solution evaporation in organic solvent. Consequently, the excitation energy predictions including solvent effects could more directly relate to relevant experimental values, so we also calculated the fundamental and optical gaps including an implicit solvent model of cyclohexane.

Table 5: The fundamental gap calculated using neutral, cation, and anion energies at different levels of theory.

	B3LYP	CAMB3LYP w/B3LYP Geometry	CAMB3LYP	CPCM Cyclohexane
1	7.435106879	8.179311458		
2	6.126102482	6.526790347	6.652479804	4.963495
3	5.045564999	5.385707499	5.530853107	3.940837
4	4.282394075	4.577556131	4.76180452	2.13702
5	3.711798228	3.986034718	4.224406582	2.731344
6	3.263844162	3.520583721		
7	2.818937772	3.182999092		

There is no experimental data providing fundamental gap calculations for Series 1 derivatives to benchmark which calculation in gas phase most closely predicts the actual value. As seen in Table 5, the lowest fundamental gaps are computed with the B3LYP level of theory, with the CAM-B3LYP energy calculations using the B3LYP optimized geometry being slightly higher, and the CAM-B3LYP energy calculations using the CAM-B3LYP optimized geometry being higher still.

For the optical gap calculations (Figure 18), the B3LYP level of theory gas-phase results for molecules 2-4 have the closest agreement with the experimental values characterized with broad UV-vis absorption peaks. This is surprising considering the B3LYP gas-phase calculations did not include the corrected physics of solvent or long-range interactions. The next "best" calculations were performed using the IPCM solvation model which have slightly larger deviations from the experimental values than the gas-phase calculations. The long-range corrected CAM-B3LYP functional calculations were higher than the experimental values, suggesting the effect of dispersions on the molecules' electronic behavior is negligible. The CPCM calculated optical gaps are significantly lower than the experimental values, suggesting this model is not recommended for calculating excitation energies in these series of molecules. More experimental data is necessary to make certain conclusions on recommendations for the best level of theory used for calculating these excitation energies. However, it is useful to know that

employing the straightforward B3LYP gas-phase optical gap calculations is sufficient for capturing trends and in good agreement with experimental optical gap excitation energies for these twisted PAHs.
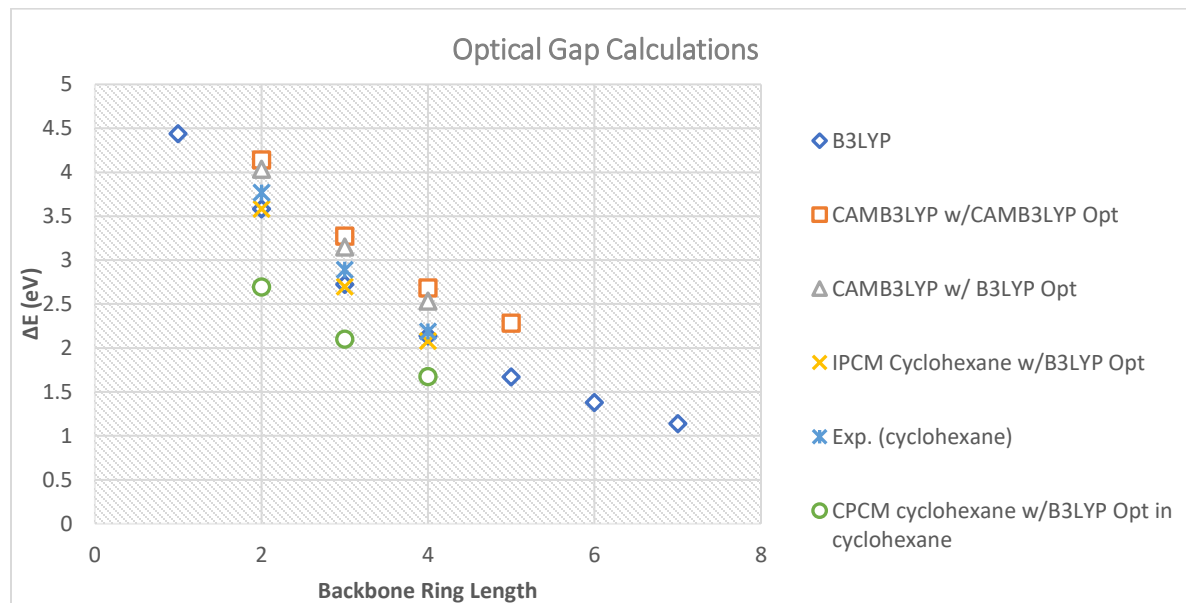

Figure 18: The theoretical optical gap calculations at various levels of theory compared with previously acquired experimental values.

Conclusion

We presented a theoretical study analyzing the effect of intramolecular geometric twist on electronic character in three families of phenyl-substituted polycyclic aromatic hydrocarbons. We first optimized the structures in the ground state at the B3LYP/6-311G level to analyze the relationship between intramolecular twist and molecular length measured by the number of rings along the fused benzene ring backbone. In all three families of twisted PAHs investigated, we found a linear relationship between backbone length and degree of twist. Using the optimized structures, we computed the HOMO-LUMO gap, fundamental gap, and optical gap in each series. We observed an approximately linear negative relationship between each excitation energy gap calculated and corresponding backbone length for all three series investigated. This decrease is expected for an increase in size for π-conjugated systems, supporting previous conclusions that intramolecular twist does not disrupt overall end-to-end electron delocalization. For Series 1 and Series 3, we found that our theoretical optical gap calculations were in agreement with UV-vis 1st singlet excitation energies. We found that the inverse relationship between molecular radius and exciton binding energy demonstrated for planar PAHs also applies to Series 1 derivatives, suggesting that the intramolecular twist may have a negligible effect on exciton binding energies. We analyzed two model systems to isolate twist effects from substituent effects on electronic character. Our results supported previous experimental and theoretical studies concluding that end-to-end intramolecular twist does not disrupt end-to-end electron delocalization. Lastly, we analyzed different levels of theory incorporating dispersion and solvent effects on the fundamental and optical gaps for Series 1 derivatives. We found the B3LYP gas-phase optical gap calculations are sufficient for capturing trends and in good agreement with experimental optical gap excitation energies for Series 1 PAHs.

References:

(1)   Lawal, A. T. Polycyclic Aromatic Hydrocarbons. A Review. *Cogent Environ. Sci.* **2017**, *3* (1), 1339841. https://doi.org/10.1080/23311843.2017.1339841.

(2)   Zou, S.-J.; Shen, Y.; Xie, F.-M.; Chen, J.-D.; Li, Y.-Q.; Tang, J.-X. Recent Advances in Organic Light-Emitting Diodes: Toward Smart Lighting and Displays. *Mater. Chem. Front.* **2020**, *4* (3), 788–820. https://doi.org/10.1039/c9qm00716d.

(3)   Aumaitre, C.; Morin, J.-F. Polycyclic Aromatic Hydrocarbons as Potential Building Blocks for Organic Solar Cells. *Chem. Rec.* **2019**, *19* (6), 1142–1154. https://doi.org/10.1002/tcr.201900016.

(4)   Wang, X.-Y.; Yao, X.; Müllen, K. Polycyclic Aromatic Hydrocarbons in the Graphene Era. *Sci. China Chem.* **2019**, *62* (9), 1099–1144. https://doi.org/10.1007/s11426-019-9491-2.

(5)   Mishra, A.; Bäuerle, P. Small Molecule Organic Semiconductors on the Move: Promises for Future Solar Energy Technology. *Angew. Chem. Int. Ed Engl.* **2012**, *51* (9), 2020–2067. https://doi.org/10.1002/anie.201102326.

(6)   Zhou, D.; Zhang, H.; Zheng, H.; Xu, Z.; Xu, H.; Guo, H.; Li, P.; Tong, Y.; Hu, B.; Chen, L. Recent Advances and Prospects of Small Molecular Organic Thermoelectric Materials. *Small* **2022**, *18* (23), e2200679. https://doi.org/10.1002/smll.202200679.

(7)   Ten Brinck, S.; Nieuwland, C.; van der Werf, A.; Veenboer, R. M. P.; Linnartz, H.; Bickelhaupt, F. M.; Fonseca Guerra, C. Polycyclic Aromatic Hydrocarbons (PAHs) in Interstellar Ices: A Computational Study into How the Ice Matrix Influences the Ionic State of PAH Photoproducts. *ACS Earth Space Chem.* **2022**, *6* (3), 766–774. https://doi.org/10.1021/acsearthspacechem.1c00433.

(8)   Lovas, F. J.; McMahon, R. J.; Grabow, J.-U.; Schnell, M.; Mack, J.; Scott, L. T.; Kuczkowski, R. L. Interstellar Chemistry: A Strategy for Detecting Polycyclic Aromatic Hydrocarbons in Space. *J. Am. Chem. Soc.* **2005**, *127* (12), 4345–4349. https://doi.org/10.1021/ja0426239.

(9)   McGuire, B. A. 2018 Census of Interstellar, Circumstellar, Extragalactic, Protoplanetary Disk, and Exoplanetary Molecules. *Astrophys. J. Suppl. Ser.* **2018**, *239* (2), 17. https://doi.org/10.3847/1538-4365/aae5d2.

(10)   Günther, A. A.; Widmer, J.; Kasemann, D.; Leo, K. Hole Mobility in Thermally Evaporated Pentacene: Morphological and Directional Dependence. *Appl. Phys. Lett.* **2015**, *106* (23), 233301. https://doi.org/10.1063/1.4922422.

(11)   Lucas, B.; El Amrani, A.; Moliton, A.; Skaiky, A.; El Hajj, A.; Aldissi, M. Charge Transport Properties in Pentacene Films: Evaluation of Carrier Mobility by Different Techniques. *Solid State Electron.* **2012**, *69*, 99–103. https://doi.org/10.1016/j.sse.2011.12.011.

(12)   Chow, T. J. Hexacene: Synthesis, Properties and Future Perspectives. *Chem. Rec.* **2015**, *15* (6), 1137–1139. https://doi.org/10.1002/tcr.201510003.

(13)   Liu, S.; Wu, H.; Zhang, X.; Hu, W. Research Progress of Rubrene as an Excellent Multifunctional Organic Semiconductor. *Front. Phys.* **2021**, *16* (1). https://doi.org/10.1007/s11467-020-0993-1.

(14)   McGarry, K. A.; Xie, W.; Sutton, C.; Risko, C.; Wu, Y.; Young, V. G., Jr; Brédas, J.-L.; Frisbie, C. D.; Douglas, C. J. Rubrene-Based Single-Crystal Organic Semiconductors: Synthesis, Electronic Structure, and Charge-Transport Properties. *Chem. Mater.* **2013**, *25* (11), 2254–2263. https://doi.org/10.1021/cm400736s.

(15)   Matsuoka, W.; Kawahara, K. P.; Ito, H.; Sarlah, D.; Itami, K. Π-Extended Rubrenes via Dearomative Annulative π-Extension Reaction. *J. Am. Chem. Soc.* **2023**, *145* (1), 658–666. https://doi.org/10.1021/jacs.2c11338.

(16) Zhang, D.; Duan, L. Polycyclic Aromatic Hydrocarbon Derivatives toward Ideal Electron-Transporting Materials for Organic Light-Emitting Diodes. *J. Phys. Chem. Lett.* **2019**, *10* (10), 2528–2537. https://doi.org/10.1021/acs.jpclett.9b00526.

(17) Li, Y.; Yu, T.; Su, W.; Wang, Y.; Zhao, Y.; Zhang, H. Polycyclic Aromatic Hydrocarbon-Bridged Coumarin Derivatives for Organic Light-Emitting Devices. *Arab. J. Chem.* **2020**, *13* (2), 4126–4133. https://doi.org/10.1016/j.arabjc.2019.05.006.

(18) Bayn, A.; Feng, X.; Müllen, K.; Haick, H. Field Effect Transistors Based on Polycyclic Aromatic Hydrocarbons for the Detection and Classification of Volatile Organic Compounds. *ACS Appl. Mater. Interfaces* **2013**, *5* (8), 3431–3440. https://doi.org/10.1021/am4005144.

(19) Pandey, M.; Kumari, N.; Nagamatsu, S.; Pandey, S. S. Recent Advances in the Orientation of Conjugated Polymers for Organic Field-Effect Transistors. *J. Mater. Chem. C Mater. Opt. Electron. Devices* **2019**, *7* (43), 13323–13351. https://doi.org/10.1039/c9tc04397g.

(20) Chen, M.; Yan, L.; Zhao, Y.; Murtaza, I.; Meng, H.; Huang, W. Anthracene-Based Semiconductors for Organic Field-Effect Transistors. *J. Mater. Chem. C Mater. Opt. Electron. Devices* **2018**, *6* (28), 7416–7444. https://doi.org/10.1039/c8tc01865k.

(21) Anthony, J. E. Functionalized Acenes and Heteroacenes for Organic Electronics. *Chem. Rev.* **2006**, *106* (12), 5028–5048. https://doi.org/10.1021/cr050966z.

(22) Anisimov, D. S.; Chekusova, V. P.; Trul, A. A.; Abramov, A. A.; Borshchev, O. V.; Agina, E. V.; Ponomarenko, S. A. Fully Integrated Ultra-Sensitive Electronic Nose Based on Organic Field-Effect Transistors. *Sci. Rep.* **2021**, *11* (1), 10683. https://doi.org/10.1038/s41598-021-88569-x.

(23) Clevenger, R. G.; Kumar, B.; Menuey, E. M.; Lee, G.-H.; Patterson, D.; Kilway, K. V. A Superior Synthesis of Longitudinally Twisted Acenes. *Chemistry* **2018**, *24* (1), 243–250. https://doi.org/10.1002/chem.201704501.

(24) Walters, R. S.; Kraml, C. M.; Byrne, N.; Ho, D. M.; Qin, Q.; Coughlin, F. J.; Bernhard, S.; Pascal, R. A., Jr. Configurationally Stable Longitudinally Twisted Polycyclic Aromatic Compounds. *J. Am. Chem. Soc.* **2008**, *130* (48), 16435–16441. https://doi.org/10.1021/ja806958x.

(25) Xiao, Y.; Mague, J. T.; Schmehl, R. H.; Haque, F. M.; Pascal, R. A., Jr. Dodecaphenyltetracene. *Angew. Chem. Int. Ed Engl.* **2019**, *58* (9), 2831–2833. https://doi.org/10.1002/anie.201812418.

(26) Vij, V.; Bhalla, V.; Kumar, M. Hexaarylbenzene: Evolution of Properties and Applications of Multitalented Scaffold. *Chem. Rev.* **2016**, *116* (16), 9565–9627. https://doi.org/10.1021/acs.chemrev.6b00144.

(27) Qiao, X.; Ho, D. M.; Pascal, R. A. An Extraordinarily Twisted Polycyclic Aromatic Hydrocarbon. *Angew. Chem. Int. Ed. Engl.* **1997**, *36* (1314), 1531–1532. https://doi.org/10.1002/anie.199715311.

(28) Lu, J.; Ho, D. M.; Vogelaar, N. J.; Kraml, C. M.; Bernhard, S.; Byrne, N.; Kim, L. R.; Pascal, R. A., Jr. Synthesis, Structure, and Resolution of Exceptionally Twisted Pentacenes. *J. Am. Chem. Soc.* **2006**, *128* (51), 17043–17050. https://doi.org/10.1021/ja065935f.

(29) Asako, T.; Suzuki, S.; Tanaka, S.; Ota, E.; Yamaguchi, J. Synthesis of Decaarylanthracene with Nine Different Substituents. *J. Org. Chem.* **2020**, *85* (23), 15437–15448. https://doi.org/10.1021/acs.joc.0c02218.

(30) Takahashi, T.; Li, S.; Huang, W.; Kong, F.; Nakajima, K.; Shen, B.; Ohe, T.; Kanno, K.-I. Homologation Method for Preparation of Substituted Pentacenes and Naphthacenes. *J. Org. Chem.* **2006**, *71* (21), 7967–7977. https://doi.org/10.1021/jo060923y.

(31) Li, S.; Jia, Z.; Nakajima, K.; Kanno, K.-I.; Takahashi, T. Dehydro Side Coupling of Substituted Pentacene Derivatives. *J. Org. Chem.* **2011**, *76* (24), 9983–9987. https://doi.org/10.1021/jo201659q.

(32) Takahashi, T.; Kitamura, M.; Shen, B.; Nakajima, K. Straightforward Method for Synthesis of Highly Alkyl-Substituted Naphthacene and Pentacene Derivatives by Homologation. *J. Am. Chem. Soc.* **2000**, *122* (51), 12876–12877. https://doi.org/10.1021/ja003130g.

(33) Tykwinski, R. R. Synthesis of Unsymmetrical Derivatives of Pentacene for Materials Applications. *Acc. Chem. Res.* **2019**, *52* (8), 2056–2069. https://doi.org/10.1021/acs.accounts.9b00216.

(34) Wolak, M. A.; Jang, B.-B.; Palilis, L. C.; Kafafi, Z. H. Functionalized Pentacene Derivatives for Use as Red Emitters in Organic Light-Emitting Diodes. *J. Phys. Chem. B* **2004**, *108* (18), 5492–5499. https://doi.org/10.1021/jp036199u.

(35) Zhou, Y.; Ma, L.; Lunchev, A. V.; Long, S.; Wu, T.; Ni, W.; Grimsdale, A. C.; Sun, L.; Gurzadyan, G. G. Switching Pathways of Triplet State Formation by Twisted Intramolecular Charge Transfer. *J. Phys. Chem. B* **2021**, *125* (45), 12518–12527. https://doi.org/10.1021/acs.jpcb.1c07045.

(36) Fleischhauer, J.; Zahn, S.; Beckert, R.; Grummt, U.-W.; Birckner, E.; Görls, H. A Way to Stable, Highly Emissive Fluorubine Dyes: Tuning the Electronic Properties of Azaderivatives of Pentacene by Introducing Substituted Pyrazines. *Chemistry* **2012**, *18* (15), 4549–4557. https://doi.org/10.1002/chem.201103350.

(37) Xiao, J.; Malliakas, C. D.; Liu, Y.; Zhou, F.; Li, G.; Su, H.; Kanatzidis, M. G.; Wudl, F.; Zhang, Q. "Clean Reaction" Strategy to Approach a Stable, Green Heptatwistacene Containing a Single Terminal Pyrene Unit. *Chem. Asian J.* **2012**, *7* (4), 672–675. https://doi.org/10.1002/asia.201100910.

(38) Fan, J.-X.; Chen, X.-K.; Zhang, S.-F.; Ren, A.-M. Theoretical Study on Charge Transport Properties of Intra- and Extra-Ring Substituted Pentacene Derivatives. *J. Phys. Chem. A* **2016**, *120* (15), 2390–2400. https://doi.org/10.1021/acs.jpca.5b12641.

(39) Wolak, M. A.; Melinger, J. S.; Lane, P. A.; Palilis, L. C.; Landis, C. A.; Delcamp, J.; Anthony, J. E.; Kafafi, Z. H. Photophysical Properties of Dioxolane-Substituted Pentacene Derivatives Dispersed in Tris(Quinolin-8-Olato)Aluminum(III). *J. Phys. Chem. B* **2006**, *110* (15), 7928–7937. https://doi.org/10.1021/jp0511045.

(40) Okamoto, T.; Senatore, M. L.; Ling, M.-M.; Mallik, A. B.; Tang, M. L.; Bao, Z. Synthesis, Characterization, and Field-Effect Transistor Performance of Pentacene Derivatives. *Adv. Mater.* **2007**, *19* (20), 3381–3384. https://doi.org/10.1002/adma.200700298.

(41) Chen, Y.; Shen, L.; Li, X. Effects of Heteroatoms of Tetracene and Pentacene Derivatives on Their Stability and Singlet Fission. *J. Phys. Chem. A* **2014**, *118* (30), 5700–5708. https://doi.org/10.1021/jp503114b.

(42) Anthony, J. E.; Eaton, D. L.; Parkin, S. R. A Road Map to Stable, Soluble, Easily Crystallized Pentacene Derivatives. *Org. Lett.* **2002**, *4* (1), 15–18. https://doi.org/10.1021/ol0167356.

(43) Norton, J. E.; Houk, K. N. Electronic Structures and Properties of Twisted Polyacenes. *J. Am. Chem. Soc.* **2005**, *127* (12), 4162–4163. https://doi.org/10.1021/ja042379l.

(44) Bedi, A.; Gidron, O. The Consequences of Twisting Nanocarbons: Lessons from Tethered Twisted Acenes. *Acc. Chem. Res.* **2019**, *52* (9), 2482–2490. https://doi.org/10.1021/acs.accounts.9b00271.

(45) Bedi, A.; Shimon, L. J. W.; Gidron, O. Helically Locked Tethered Twistacenes. *J. Am. Chem. Soc.* **2018**, *140* (26), 8086–8090. https://doi.org/10.1021/jacs.8b04447.

(46) Clevenger, R. G.; Kumar, B.; Menuey, E. M.; Kilway, K. V. Synthesis and Structure of a Longitudinally Twisted Hexacene. *Chemistry* **2018**, *24* (13), 3113–3116. https://doi.org/10.1002/chem.201705676.

(47) Becke, A. D. Density-functional Thermochemistry. III. The Role of Exact Exchange. *J. Chem. Phys.* **1993**, *98* (7), 5648–5652. https://doi.org/10.1063/1.464913.

(48) Lee, C.; Yang, W.; Parr, R. G. Development of the Colle-Salvetti Correlation-Energy Formula into a Functional of the Electron Density. *Phys. Rev. B Condens. Matter* **1988**, *37* (2), 785–789. https://doi.org/10.1103/physrevb.37.785.

(49) Vosko, S. H.; Wilk, L.; Nusair, M. Accurate Spin-Dependent Electron Liquid Correlation Energies for Local Spin Density Calculations: A Critical Analysis. *Can. J. Phys.* **1980**, *58* (8), 1200–1211. https://doi.org/10.1139/p80-159.

(50) Stephens, P. J.; Devlin, F. J.; Chabalowski, C. F.; Frisch, M. J. Ab Initio Calculation of Vibrational Absorption and Circular Dichroism Spectra Using Density Functional Force Fields. *J. Phys. Chem.* **1994**, *98* (45), 11623–11627. https://doi.org/10.1021/j100096a001.

(51) Marenich, A. V.; Cramer, C. J.; Truhlar, D. G. Universal Solvation Model Based on Solute Electron Density and on a Continuum Model of the Solvent Defined by the Bulk Dielectric Constant and Atomic Surface Tensions. *J. Phys. Chem. B* **2009**, *113* (18), 6378–6396. https://doi.org/10.1021/jp810292n.

(52) Yanai, T.; Tew, D. P.; Handy, N. C. A New Hybrid Exchange–Correlation Functional Using the Coulomb-Attenuating Method (CAM-B3LYP). *Chem. Phys. Lett.* **2004**, *393* (1–3), 51–57. https://doi.org/10.1016/j.cplett.2004.06.011.

(53) Malloci, G.; Cappellini, G.; Mulas, G.; Mattoni, A. Electronic and Optical Properties of Families of Polycyclic Aromatic Hydrocarbons: A Systematic (Time-Dependent) Density Functional Theory Study. *Chem. Phys.* **2011**, *384* (1–3), 19–27. https://doi.org/10.1016/j.chemphys.2011.04.013.

(54) Bredas, J.-L. Mind the Gap! *Mater. Horiz.* **2014**, *1* (1), 17–19. https://doi.org/10.1039/c3mh00098b.

(55) Mocci, P.; Malloci, G.; Bosin, A.; Cappellini, G. Time-Dependent Density Functional Theory Investigation on the Electronic and Optical Properties of Poly-C,Si,Ge-Acenes. *ACS Omega* **2020**, *5* (27), 16654–16663. https://doi.org/10.1021/acsomega.0c01516.

(56) Nayak, P. K. Exciton Binding Energy in Small Organic Conjugated Molecule. *Synth. Met.* **2013**, *174*, 42–45. https://doi.org/10.1016/j.synthmet.2013.04.010.

(57) Qiao, X.; Padula, M. A.; Ho, D. M.; Vogelaar, N. J.; Schutt, C. E.; Pascal, R. A. Octaphenylnaphthalene and Decaphenylanthracene. *J. Am. Chem. Soc.* **1996**, *118* (4), 741–745. https://doi.org/10.1021/ja953669s.

(58) Lu, J.; Ho, D. M.; Vogelaar, N. J.; Kraml, C. M.; Pascal, R. A., Jr. A Pentacene with a 144 Degrees Twist. *J. Am. Chem. Soc.* **2004**, *126* (36), 11168–11169. https://doi.org/10.1021/ja046576w.